5-1995

Dynamic Reaction Coordinate Analysis: An Application to SiH4 + H- → SiH5-

Tetsuya Taketsugu
Iowa State University

Mark S. Gordon
Iowa State University, mgordon@iastate.edu

Dynamic Reaction Coordinate Analysis: An Application to SiH4 + H- → SiH5-

Abstract
An ab initio classical trajectory method, the dynamic reaction coordinate (DRC) method based on ab initio electronic structure calculations, is applied to a study of the chemical reaction Si~ + H- - SiHs-. Both side attack (C2v symmetry) and front attack (C3v symmetry) of H- on SiH4 are examined. To analyze the nature of the intramolecular vibrational energy transfer, the DRC and its corresponding momentum are mapped onto normal modes of both reactant and product systems. These analyses show that Berry pseudorotation occurs repeatedly in the SiH5- produced by the side attack, whereas the SN2 reaction H- + Si~ - Si~ + H- often occurs upon front attack depending on the initial relative velocity.

Disciplines
Chemistry

ARTICLES

Dynamic Reaction Coordinate Analysis: An Application to $SiH_4 + H^- \rightarrow SiH_5^-$

Tetsuya Taketsugu and Mark S. Gordon*

Department of Chemistry, Iowa State University, Ames, Iowa 50011

Received: January 11, 1995; In Final Form: March 13, 1995[⊗]

An *ab initio* classical trajectory method, the dynamic reaction coordinate (DRC) method based on *ab initio* electronic structure calculations, is applied to a study of the chemical reaction $SiH_4 + H^- \rightarrow SiH_5^-$. Both side attack ($C_{2v}$ symmetry) and front attack (C_{3v} symmetry) of H^- on SiH_4 are examined. To analyze the nature of the intramolecular vibrational energy transfer, the DRC and its corresponding momentum are mapped onto normal modes of both reactant and product systems. These analyses show that Berry pseudorotation occurs repeatedly in the SiH_5^- produced by the side attack, whereas the S_N2 reaction $H^- + SiH_4 \rightarrow SiH_4 + H^-$ often occurs upon front attack depending on the initial relative velocity.

I. Introduction

Pentacoordinated silicon anions have been the subject of both experimental[1−5] and theoretical[6−17] interest, due to their implication in a variety of chemical reactions. Of particular interest has been the nature of isomerization of such species by the Berry pseudorotation process[18] and the manner in which pseudorotation affects reactivity. Since the barrier to pseudorotation is generally much smaller than the well corresponding to $SiH_4 + X^- \rightarrow SiH_4X^-$, pseudorotation within the well can have an impact on the subsequent chemistry. The equilibrium structure of the simplest pentacoordinated silicon anion, SiH_5^-, is trigonal bipyramidal. Berry pseudorotation (Figure 1) proceeds from one trigonal bipyramidal arrangement to another through a tetragonal transition state with a 2 (3) kcal/mol barrier at the second-order perturbation theory (Hartree−Fock) level of theory.[11] This process of pseudorotation from trigonal bipyramid through the transition state may be used as a prototype to study the dynamical behavior of SiH_5^-. A particularly interesting question is what is the nature of the intramolecular vibrational energy transfer between the initial approach of H^- (that presumably becomes the Si−H stretching motion) and the pseudorotation?

There are many ways in which an H^- may approach SiH_4. However, three attack orientations upon a highly symmetrical SiH_4 are side, front, and back attack as shown in Figure 2. Due to the molecular symmetry, these attacks may occur in six, four, and four equivalent ways, respectively. The expected products are SiH_5^- (addition) in side or front attack, $SiH_4 + H^-$ (S_N2) in front attack, and $SiH_3^- + H_2$ (abstraction) in back attack. It should be noted that, in the addition reaction, the H^- anion is likely to occupy an equatorial position in side attack vs an axial position in front attack (see Figure 2). In this paper, we study the side and front attack cases.

When a chemical reaction is studied in quantum chemistry, typically stationary points, *i.e.*, reactant, product, and transition state geometries, are located and then the character of these stationary points is determined by normal mode analysis. Once these stationary points have been characterized, the reaction path may be followed, using the intrinsic reaction coordinate (IRC)[19]

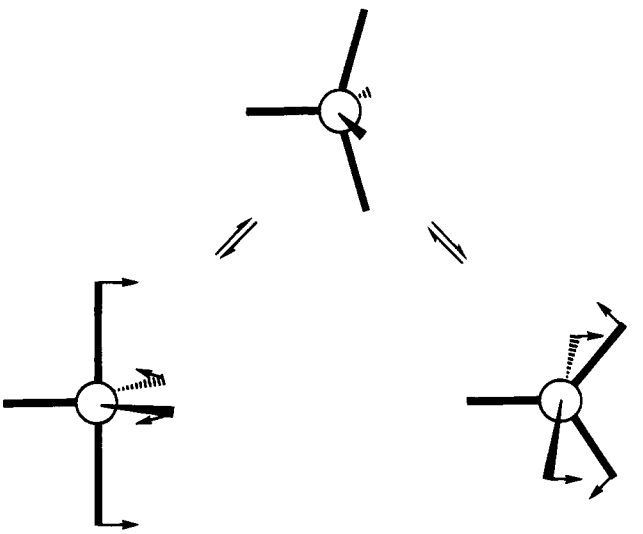

Figure 1. Illustration of Berry pseudorotation.

method, from transition state to both reactants and products. More detailed dynamic information may be obtained by determining the reaction path Hamiltonian.[20] The vibrational normal modes can be defined systematically along the reaction path by diagonalizing the Hessian matrix of energy second derivatives after projecting out the gradient vector (the reaction coordinate direction). This approach probes small vibrational displacements transverse to the minimum energy path. Recently, Hirano *et al.*[21,22] proposed useful methods that make use of vibration mixing and vibration mapping to describe a vibrationally interacting system using reactant and product normal modes. Their scheme suggests that the correlation diagram connecting normal modes from reactant to product is helpful in the same manner as a molecular orbital (MO) diagram because those modes belonging to different symmetry representations cannot mix with each other throughout the reaction. These are all, however, static analyses in the sense that they examine static features of a potential surface which governs the molecular dynamical process.

For the examination of dynamical aspects of a reaction directly with *ab initio* wave functions, one can turn to the dynamic reaction coordinate (DRC) approach.[23−25] The DRC

[⊗] Abstract published in *Advance ACS Abstracts,* May 1, 1995.

0022-3654/95/2099-8462$09.00/0

Side attack (C_{2v} symmetry)

Front attack (C_{3v} symmetry)

Back attack (C_{3v} symmetry)

Figure 2. Illustration of side, front, and back attack of H^- to SiH_4.

method was introduced originally by Stewart *et al.*[23] and was used to calculate IRC paths efficiently on the (semiempirical) MNDO[26] potential surface for reactions $SiX_6^{2-} \rightarrow SiX_5^- + X^-$ (X = F, OH). Dupuis *et al.*[24] implemented this scheme into the *ab initio* MO program package HONDO[27] and applied it to predict the IRC path of the 1,5-hexadiene Cope rearrangement. Most recently, Taketsugu *et al.*[25] implemented this DRC scheme into the electronic structure program package GAMESS[28] and applied the method to intramolecular vibrational mixing in H_2O. The DRC method may be thought of as a classical trajectory calculation "on-the-fly" since one does not need to determine the potential energy surface for the process of interest prior to the trajectory calculation. The negative of the energy gradient (force on the atoms) is used to obtain atomic accelerations, velocities, and positions. Thus, it is not necessary to separately construct the potential surface; all degrees of freedom are automatically contained in the calculations.

To our knowledge, few applications using *ab initio* trajectories have been reported.[25,29,30] This is partly because a DRC calculation requires more computing time than does a typical classical trajectory calculation. However, the increased efficiency of both software and hardware makes such calculations increasingly feasible.

In this paper, to analyze the energy transfer process among various modes upon the reaction of H^- with SiH_4 (*i.e.*, translation, rotation, and vibration), we perform a mapping of DRCs and their corresponding conjugate momenta simultaneously onto both reactant and product normal modes. In other words, we adopt the normal modes of the reactant and product as basis vectors (basis sets) to describe the reaction dynamics. A normal mode is a special basis vector in the sense that its physical meaning is that of a normal vibration relative to the equilibrium geometry. (It should be noted that, when the reaction system stays far from equilibrium, the description in terms of normal modes loses its physical meaning as a vibration.) This approach is based on the fact that reactants with internal motions become products with internal motions through a complicated energy transfer process in a chemical reaction. This analysis makes it possible to understand the dynamics of a reaction from two viewpoints (reactant and product) and thus provides information about energy transfer.

II. Methods of Calculation

Ab initio MO calculations are performed for the reaction, $SiH_4 + H^- \rightarrow SiH_5^-$, with the 6-31++G(d,p)[31] basis set, using the restricted Hartree–Fock (RHF) method. It has previously been shown[9-11] that the effect of correlation on this reaction is small enough that RHF calculations provide a qualitatively reasonable picture. The equilibrium geometries are located for reactants and product, and normal mode analysis is performed for both structures. For both side attack (C_{2v} symmetry) and front attack (C_{3v} symmetry) paths, energy profiles are calculated as a function of the $Si-H^-$ distance such that the other geometrical parameters are optimized under symmetry constraints.

DRC calculations are performed for both side and front attack processes at the same computational level. As initial conditions, it is assumed that an H^- attacks equilibrium SiH_4 along the principal axis of symmetry of the reaction system, *i.e.*, C_{2v} and C_{3v} symmetry in side and front attack cases, respectively. With these conditions, the reaction system is constrained to the initial symmetry, because the DRC calculation is based on Newton's equations, so the initial symmetry must be retained. Thus, these processes can be described only in terms of the totally symmetric coordinates. It should be noted that due to this symmetry constraint Berry pseudorotation can only be initiated in a side attack (see Figures 1 and 2).

To analyze the process of energy transfer among vibrational modes, the DRCs and their conjugate momenta transformed into mass-weighted coordinates are mapped onto totally symmetric normal modes of the reactant (R) and product (P) as follows,[25]

$$Q_i^{\mathrm{A}}(t) = \sum_k^{3N} (X_k(t) - X_k^{\mathrm{A}})\sqrt{m_k} L_{ki}^{\mathrm{A}} \tag{1}$$

$$P_i^{\mathrm{A}}(t) = \sum_k^{3N} \dot{X}_k(t)\sqrt{m_k} L_{ki}^{\mathrm{A}} \quad (\mathrm{A} = \mathrm{R\ or\ P}) \tag{2}$$

where Q_i^{A} and P_i^{A} are the ith normal coordinate and its conjugate momentum, respectively, X_k and $\dot{X}_k$ are the kth Cartesian coordinate and corresponding velocity, respectively, X_k^{A} is the kth Cartesian coordinate of the equilibrium geometry (R or P), L_{ki}^{A} is the kth component of the ith normal mode, m_k is the atomic mass corresponding to X_k, and N is the number of atoms in the reaction system. Then, we have two representations, $(Q_i^{\mathrm{R}}(t), P_i^{\mathrm{R}}(t))$ and $(Q_i^{\mathrm{P}}(t), P_i^{\mathrm{P}}(t))$, for the DRC trajectory. The former shows harmonic vibrations when $\mathbf{X}(t)$ stays in the region around $\mathbf{X}^{\mathrm{R}}$ while the latter shows harmonic vibrations when $\mathbf{X}(t)$ approaches the region of $\mathbf{X}^{\mathrm{P}}$.

All calculations are performed using the electronic structure program package, GAMESS.[28]

III. Results and Discussion

A. Potential Energy Surface of Reaction System. Figure 3 shows energy profiles as a function of the $Si-H^-$ distance, r, along the (a) C_{2v} (side attack) and (b) C_{3v} (front attack) optimized path, respectively. The energies are given relative to the dissociation limit ($SiH_4 + H^-$). The energy minimum points at $r = 1.52$ Å in (a) and $r = 1.63$ Å in (b) correspond to the product, SiH_5^-. As is shown in these figures, the former profile has both an energy minimum and maximum between separated

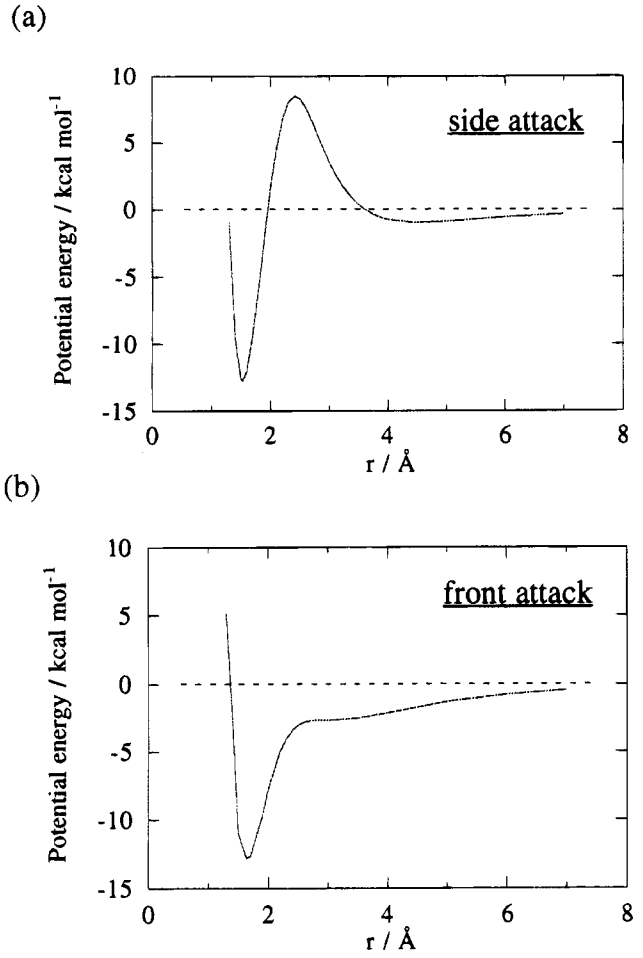

Figure 3. Energy profiles as a function of the Si-H$^-$ distance, r, along the (a) C_{2v} (side attack) and (b) C_{3v} (front attack) optimized path, respectively. The energies are relative to the dissociation limit.

TABLE 1: Energy Values (kcal/mol) Relative to the Dissociation Limit ($SiH_4 + H^-$) Calculated by RHF and MP2 Methods

	SiH_5^-	max (C_{2v})	min (C_{2v})	$r = 3$ Å (C_{3v})
RHF	−12.8	8.5	−0.9	−2.7
MP2	−19.1	4.9	−1.3	−4.1

reactants and the product, while the latter is downhill to product, with a very flat region around $r = 3$ Å. In order to examine the effect of electron correlation, we also performed MP2 calculations at the RHF optimized geometry of the product, the minimum ($r = 4.46$ Å) and maximum ($r = 2.42$ Å) points (side attack), and the geometry optimized at $r = 3$ Å (front attack). The calculated energy values relative to that of the dissociation limit are given in Table 1. The RHF and MP2 surfaces are quantitatively a bit different but qualitatively similar. Thus, in this study, the DRC at the HF level is expected to be sufficient to obtain a qualitative analysis of the dynamics.

A normal mode analysis at the energy maximum and minimum points on the side attack path shows that those structures correspond to a second-order saddle point (two imaginary modes) and a transition state, respectively. Both structures have a nontotally symmetric mode with an imaginary frequency that breaks the C_{2v} symmetry in a direction toward the front attack path. This suggests that the side attack path is unfavorable, so that when the H$^-$ anion approaches SiH_4 from the side, the H$^-$ turns away from the side attack path. Only when the initial relative velocity of H$^-$ and SiH_4 is sufficiently large can the H$^-$ attack along the side direction before turning aside.

TABLE 2: Vibrational Frequency ν (cm^{-1}) and Period τ (fs) of Normal Modes, L_i, of SiH_4 (T_d Symmetry) and SiH_5^- (D_{3h} Symmetry). Each Symmetry Representation Is Also Given

SiH_4	L_1	L_2,L_3	L_4,L_5,L_6	L_7,L_8,L_9
symmetry	A_1	E	T_2	T_2
frequency ν	2360	1051	2351	1012
period τ	14.1	31.7	14.2	32.9

SiH_5^-	L_1	L_2	L_3	L_4	L_5,L_6	L_7,L_8	L_9,L_{10}	L_{11},L_{12}
symmetry	A_1'	A_1'	A_2'	A_2''	E′	E′	E′	E″
frequency ν	2082	1346	1534	1012	2041	1100	600	1277
period τ	16.0	24.8	21.7	32.9	16.3	30.3	55.6	26.1

In the initial stage of the DRC calculations, the H$^-$ is located at 7 Å away from the Si in both attack cases. The potential energies for the initial structures are calculated to be −0.3 and −0.4 kcal/mol in side and front attacks, respectively. For the side attack, the reaction system needs more than 8.8 (=8.5 + 0.3) kcal/mol (see Table 1) to cross the maximum. In contrast, for a front attack, the reaction system in principle needs no kinetic energy because the energy profile is downhill to product as shown in Figure 3b. Four initial kinetic energies are studied for each attack direction: 9, 10, 11, and 13 kcal/mol for the side attack and 1, 3, 5, and 7 kcal/mol for the front attack. The time step is taken as 0.1 fs, and a trajectory of >400 fs is calculated in every case.

B. Normal Modes of Reaction System. Table 2 gives the symmetry representation, vibrational frequency (cm^{-1}), and period (fs) of each normal mode in SiH_4 (T_d symmetry) and SiH_5^- (D_{3h} symmetry). In SiH_4, modes with low frequency ($\mathbf{L}_2$, $\mathbf{L}_3$, $\mathbf{L}_7$, $\mathbf{L}_8$, and $\mathbf{L}_9$) are primarily H−Si−H bending, and modes with high frequency ($\mathbf{L}_1$, $\mathbf{L}_4$, $\mathbf{L}_5$, and $\mathbf{L}_6$) are primarily Si−H stretching. In SiH_5^-, the five highest frequency modes are Si−H stretches, with $\mathbf{L}_2$ and $\mathbf{L}_3$ being primarily axial stretches and $\mathbf{L}_1$, $\mathbf{L}_5$, and $\mathbf{L}_6$ being primarily equatorial stretches. Modes $\mathbf{L}_4$, $\mathbf{L}_7$, $\mathbf{L}_8$, $\mathbf{L}_{11}$, and $\mathbf{L}_{12}$ are dominated by H_{ax}−Si−H_{eq} bending motions, whereas $\mathbf{L}_9$ and $\mathbf{L}_{10}$ correspond to the H_{eq}−Si−H_{eq} bend as reported by Gordon *et al.*[11]

The molecules SiH_4 and SiH_5^- have 9 and 12 normal modes, respectively. When the H$^-$ anion approaches SiH_4, the supermolecule (H$^-$···SiH_4) acquires a symmetry that depends on the direction of H$^-$ approach (giving a subgroup of the original SiH_4 T_d symmetry). Since the supermolecule is composed of six atoms, it has 12 normal modes even when two fragments are so separated that they have no interaction with each other.

Based on the vibrational correlation method proposed by Hirano *et al.*,[21,22] the 12 modes of the supermolecule can be understood as a combination of modes of H$^-$ and SiH_4. When the interaction of H$^-$ and SiH_4 is weak (or they are well-separated), nine modes originate from SiH_4 and three modes originate from H$^-$ translations and SiH_4 translations or rotations. Note that the latter three modes have zero eigenvalues. One of these three is the mode resulting in H$^-$−SiH_4 collision, $\mathbf{L}_{col}$. The mode $\mathbf{L}_{col}$ can be expressed as[21,22]

$$\mathbf{L}_{col} = \left(\frac{m_{H^-}}{m_{SiH_4} + m_{H^-}}\right)^{1/2} \mathbf{T}_{SiH_4,z} - \left(\frac{m_{SiH_4}}{m_{SiH_4} + m_{H^-}}\right)^{1/2} \mathbf{T}_{H^-,z} \quad (3)$$

where m_X is the mass of fragment X and $\mathbf{T}_{X,z}$ is a translation of X along the z-axis in mass-weighted coordinates[32] (it is assumed that the two fragments collide with each other along the z-axis). Naturally, all modes should be classified according to symmetry representations of the supermolecule. Note that, in the supermolecule, the degenerate modes in SiH_4 are split depending on the direction of H$^-$ approach even when the fragments are far enough apart that their frequencies remain the same.

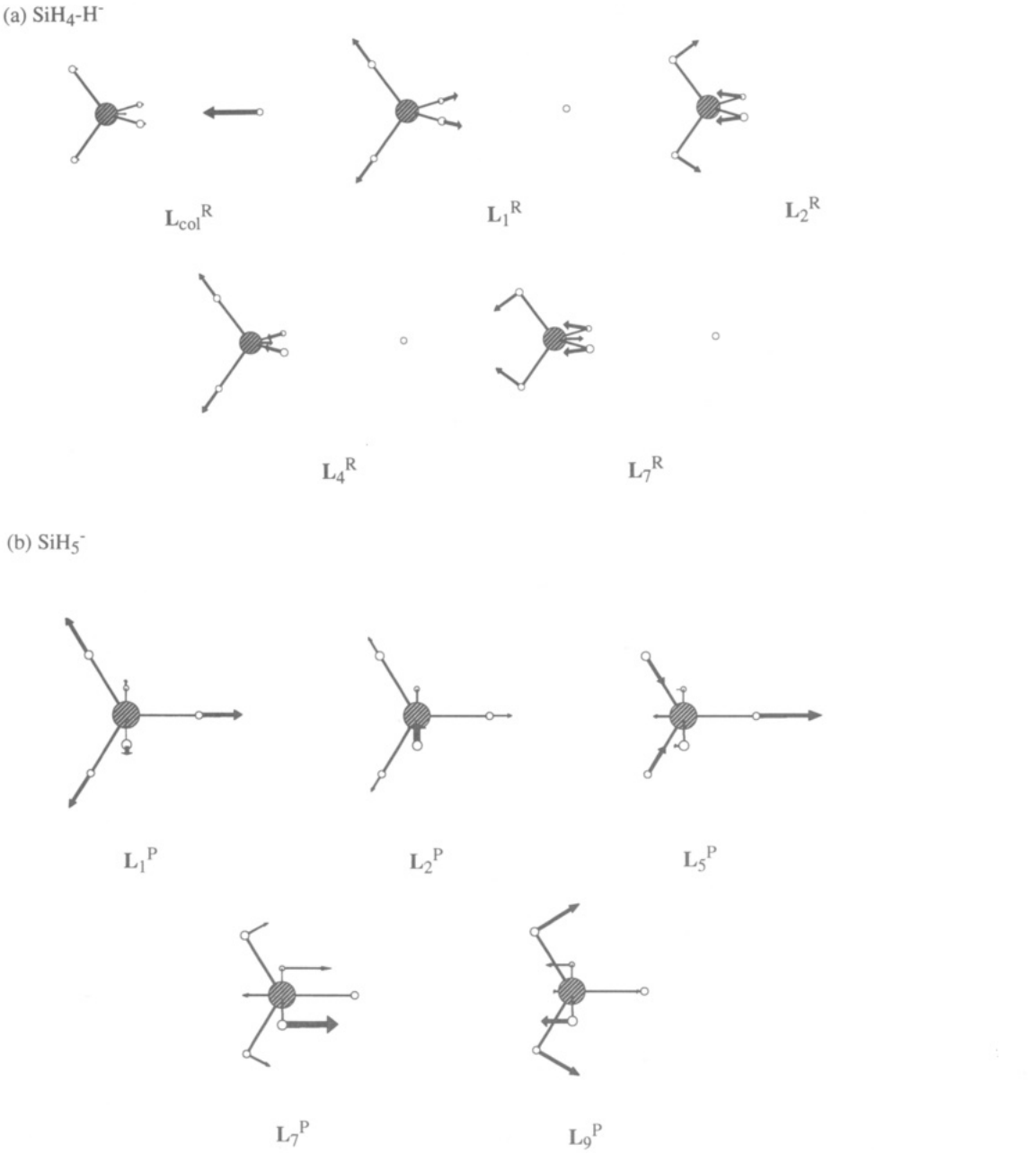

Figure 4. Basis modes in side attack: (a) reactant and (b) product.

In these DRC calculations, the normal modes of both reactant and product are adopted as coordinate basis vectors to describe molecular dynamics, *i.e.*, two coordinate systems are prepared for the description. The origins of these coordinate systems are located at the starting point, where H^- is 7 Å separated from the equilibrium SiH_4, and at equilibrium SiH_5^-. The supermolecule normal modes ($H^-\cdots SiH_4$) are employed as basis modes for the reactants. Since the reaction system never loses its symmetry during the DRC calculation, the reaction process can be described only in terms of totally symmetric coordinates, *i.e.*, totally symmetric normal modes. Of course, the set of totally symmetric normal modes in the (C_{2v}) side attack is different from that in the (C_{3v}) front attack. In the following, basis modes of the side and front attack are separately described with illustrations.

1. Side Attack. In the side attack, there are five totally symmetric normal modes. Thus, this process is described in a five-dimensional configuration space. Parts a and b of Figure 4 show the basis modes for the reactants and product, respectively. The superscripts R and P denote reactant and product, respectively. In Figure 4a, the distance between H^- and Si is scaled for convenience. The positive direction of each mode is indicated by the arrows. The numbering of the normal modes is the same as that given in Table 2, and $\mathbf{L}_{col}^R$ is defined in eq 3. According to Table 2, the basis modes originate from A_1, E, and T_2 modes in SiH_4 and A_1' and E′ modes in the product. $\mathbf{L}_2^R$, $\mathbf{L}_4^R$, and $\mathbf{L}_7^R$ in the reactant and $\mathbf{L}_5^P$, $\mathbf{L}_7^P$, and $\mathbf{L}_9^P$ in the product originate from degenerate modes.

In the initial stage of a DRC calculation, the reaction system is located at the origin ($\mathbf{Q}^R(0) = 0$) and has kinetic energy only in the direction of $\mathbf{L}_{col}^R$ ($P_i^R(0) = 0$ when $i \neq$ col) in the reactant coordinate space. As the H^- approaches SiH_4, the other modes in Figure 4a ($\mathbf{L}_1^R$, $\mathbf{L}_2^R$, $\mathbf{L}_4^R$, and $\mathbf{L}_7^R$) may be excited by acquiring energy from $\mathbf{L}_{col}^R$. When mode $\mathbf{L}_2^R$ is excited, it leads to Berry pseudorotation.

When this process is described using the coordinate system of the product (Figure 4b), as H^- approaches SiH_4, the reaction system approaches the origin. The initial kinetic energy in this case is distributed among all product modes, $\mathbf{L}_1^P$, $\mathbf{L}_2^P$, $\mathbf{L}_5^P$, $\mathbf{L}_7^P$, and $\mathbf{L}_9^P$. The momentum of each mode is determined in

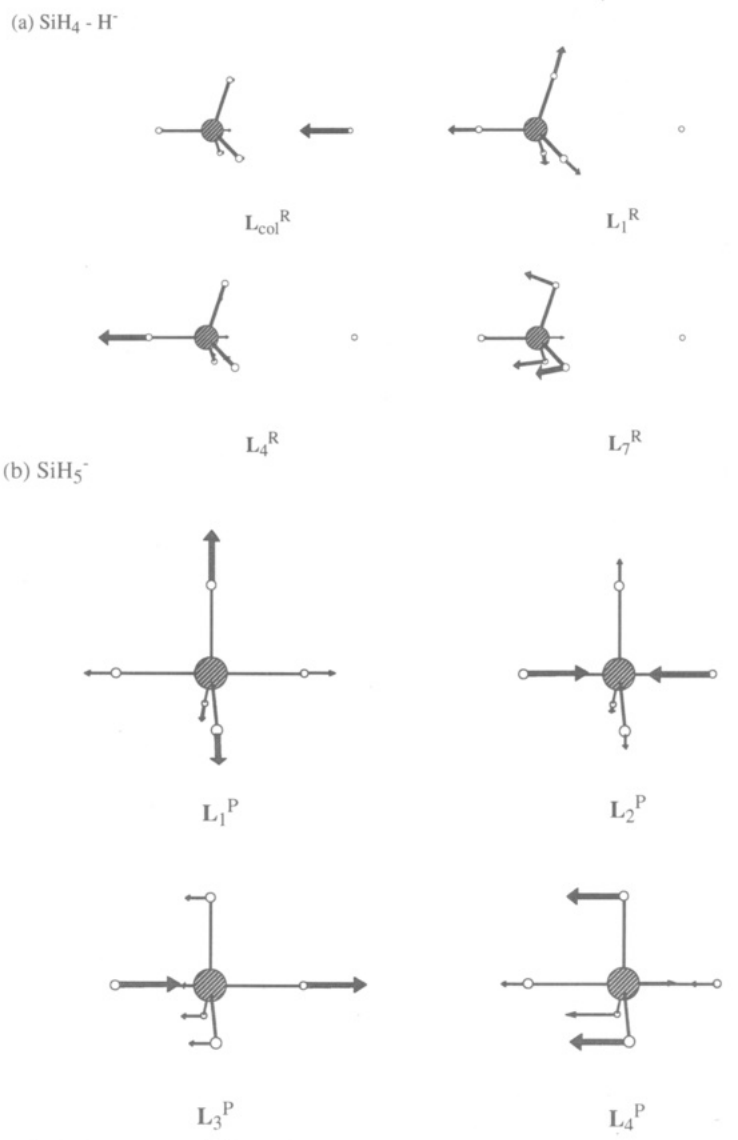

Figure 5. Basis modes in front attack: (a) reactant and (b) product.

proportion to the magnitude of its projection onto $\mathbf{L}_{col}^R$, *i.e.*, $(\mathbf{L}_i^P \cdot \mathbf{L}_{col}^R)$. $\mathbf{L}_9^P$ is the mode leading to Berry pseudorotation. Thus, it is of interest to examine the interaction between $\mathbf{L}_{col}^R$ and $\mathbf{L}_2^R$ in the reactant and to examine the motions along $\mathbf{L}_9^P$ in the product.

2. Front Attack. In the front attack, we have four totally symmetric normal modes to describe the process. Parts a and b of Figure 5 show these basis modes in the reactants and product, respectively. The basis modes originate from A_1 and T_2 modes (Table 2) in SiH_4 and A_1', A_2', and A_2'' modes in the product. In the reactant, $\mathbf{L}_4^R$ and $\mathbf{L}_7^R$ originate from degenerate modes (T_2). Note that, since the splitting of degenerate modes is different, $\mathbf{L}_4^R$ and $\mathbf{L}_7^R$ in the reactant are different from those in the side attack case (compare those in Figure 5a with those in Figure 4a).

As noted for the side attack, the reaction system starts from the origin in the direction of $\mathbf{L}_{col}^R$ in the reactant coordinate space. As H^- approaches SiH_4, modes $\mathbf{L}_1^R$, $\mathbf{L}_4^R$, and $\mathbf{L}_7^R$ (Figure 5a) may be excited. When $\mathbf{L}_4^R$ and $\mathbf{L}_7^R$ are excited, an S_N2 reaction can occur. In the product coordinate system (Figure 5b), $\mathbf{L}_4^P$ denotes the movements leading to the S_N2 reaction. Thus, it is of interest to examine the interactions among $\mathbf{L}_{col}^R$, $\mathbf{L}_4^R$, and $\mathbf{L}_7^R$ in the reactant and to examine the motions along $\mathbf{L}_4^P$ in the product.

C. DRC Analysis. *1. Side Attack.* Figure 6 shows the potential energy changes along the DRC trajectory in the side attack; the initial kinetic energy is taken to be (a) 9, (b) 10, (c) 11, and (d) 13 kcal/mol. Since the DRC method conserves the total energy, the sum of potential and kinetic energy is constant. As an example, the kinetic energy change is also shown in case a. The bottom of the potential energy well (global minimum) is −12.8 kcal/mol (Table 1). This is indicated by the dashed line in Figure 6.

In the first stage, the potential energy decreases slowly over 25−30 fs depending on the initial velocities and then starts to increase rapidly. In this stage, the H^- approaches SiH_4 from $r = 7$ Å to $r = 4$ Å in Figure 3a. It should be noted that, in the absence of symmetry constraints, the reaction system would lose C_{2v} symmetry in this region as discussed earlier and deviate from the side attack path. For case a after about 20−35 fs, the potential attains a maximum of 9 kcal/mol and then hardly changes beyond ∼100 fs.

In case (a), the potential fluctuations settle down around 0 kcal/mol and show only slight vibrational motion after that. This means that the reaction system cannot cross the maximum in Figure 3a and is again separated into two fragments, *i.e.*, H^- and SiH_4. As was described in the previous section, the reaction system needs more than 8.8 kcal/mol to cross the maximum. However, dynamically, some energy will be transferred to the other vibration modes through vibrational interactions. So, the kinetic energy of 9 kcal/mol is not enough to cross over the pass. In the other cases (b)−(d), after crossing over the pass

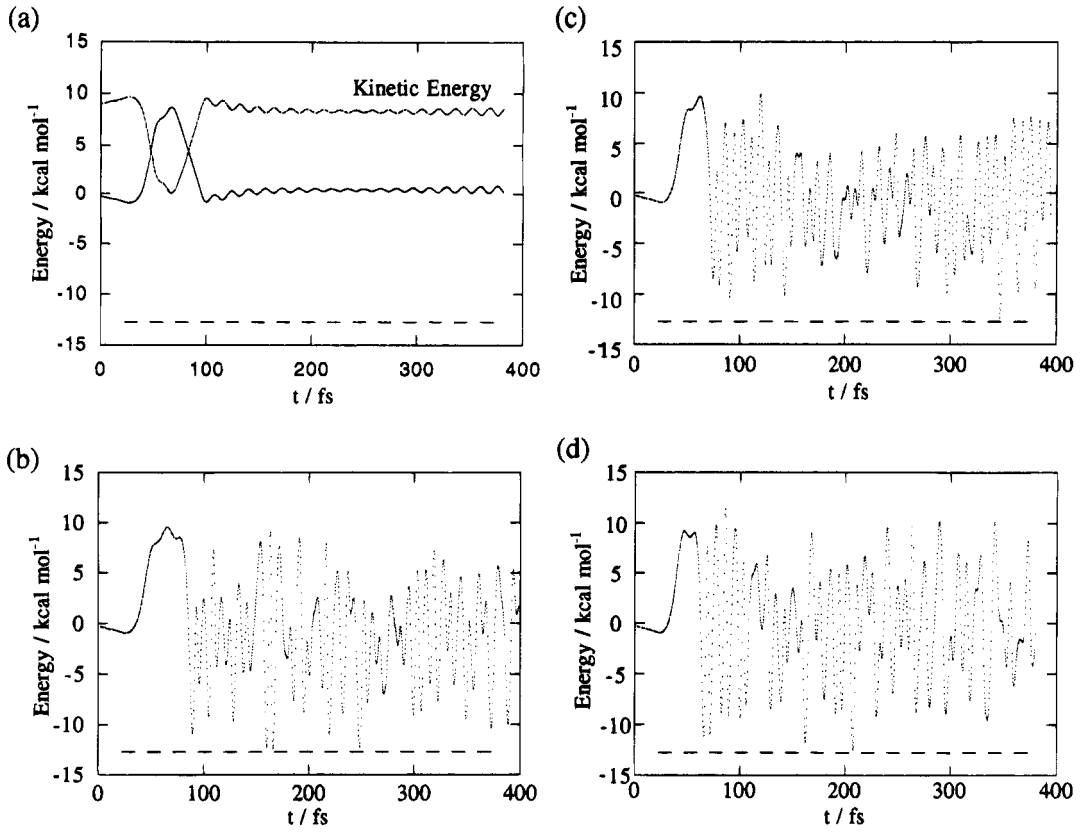

Figure 6. Potential energy changes along the DRC trajectory in side attack; the initial kinetic energy is (a) 9, (b) 10, (c) 11, and (d) 13 kcal/mol. The kinetic energy change is also given in case a. The dashed line shows the potential energy well (global minimum).

of about 10 kcal/mol, vibrational structure can be seen in the potential profiles. Thus, the reaction system crosses over the pass and comes into the well of SiH_5^-.

Next, consider the DRC analysis in terms of the basis modes of the reactant given in Figure 4a. Figure 7 shows changes of those normal coordinates along the DRC trajectory. Each part of Figure 7 corresponds to parts (a)−(d) of Figure 6, respectively. In this coordinate system, the reaction system is initially located at the origin, and is deformed into the positive direction of $\mathbf{L}_{col}^R$. Around t = 50 fs (or Q_{col}^R = 8 bohr amu$^{1/2}$), the other modes begin to fluctuate. For case a, corresponding to the smallest input of kinetic energy, Q_{col}^R decreases sharply after 80 fs. For cases (b)−(d), after about 50−70 fs, Q_{col}^R fluctuates around Q_{col}^R = 10 bohr amu$^{1/2}$ (see also Figure 6). In this period, for (b)−(d) some of the initial translational energy is used for the geometrical deformation of SiH_4 to that in SiH_5^-. In case (a), due to the insufficient kinetic energy, the H^- is scattered (Q_{col}^R decreases with a constant rate after that). It should be noted that, in case (a), the vibrational modes of SiH_4 obtain a small amount of energy from the H^- attack and show some vibrational motion after the scattering.

In the other cases, *i.e.*, (b)−(d), all modes show a large fluctuation. The most characteristic feature is the fluctuation of the pair of modes $\mathbf{L}_1^R$ and $\mathbf{L}_2^R$ with a constant ratio. As noted above, $\mathbf{L}_2^R$ in Figure 4a corresponds to Berry pseudorotation. So, in the SiH_5^- complex produced by the side attack, Berry pseudorotation appears to occur repeatedly. Judging from parts (b)−(d) of Figure 7, another trigonal-bipyramidal geometry connected by pseudorotation is located at about (Q_1^R, Q_2^R) = (−3, 4).

Since pseudorotation is an SiH_5^- mode, the above dynamics can be seen directly in terms of the product basis modes given in Figure 4b. Parts (a)−(d) of Figure 8, corresponding to parts (a)−(d) of Figure 7, illustrate the changes of those normal coordinates along the DRC trajectory. In the initial stage, all coordinates go toward zero, meaning that the reaction system goes toward equilibrium SiH_5^-. For cases (b)−(d) after approaching the origin, each mode exhibits a fluctuation about 0, with some fluctuations (*e.g.*, $\mathbf{L}_9^P$) being quite large. In addition, it can be verified that the fluctuations of $\mathbf{L}_9^P$ (Berry pseudorotation) causes changes of the vibrational center of this mode periodically between Q_9^P = 0 and 3 bohr amu$^{1/2}$. Thus, this complex oscillates between two equilibrium structures.

In summary, Berry pseudorotation occurs continuously within the well of SiH_5^- produced by the side attack of H^-, and thus, SiH_5^- is very active dynamically.

2. Front Attack. Figure 9 shows changes in the potential energy along the DRC trajectory for the front attack; the kinetic energies initially given to the system are (a) 1, (b) 3, (c) 5, and (d) 7 kcal/mol. As before, the dashed line indicates the global minimum corresponding to the product. The potential energy decreases gradually over about 50−100 fs, whereupon it falls into the product well. The larger the initial velocity is, the faster the reaction system drops into the well. Since the reaction system may deviate from the optimized path, it does not necessarily arrive at the bottom of the well.

After entering the well, each trajectory undergoes violent fluctuations of the potential energy. The larger the initial velocity, the more violent the fluctuation. The potential often goes beyond the dissociation limit. After about t = 300 fs, the fluctuations of the potential energy moderate, and the trajectory settles into slight vibration around zero in cases (a) and (b). In case (d), the fluctuation of the potential energy also acquires a constant rhythm after about t = 300 fs, but the magnitude of the fluctuations is large and the center of the vibration is not at the origin. The results for (a) and (b) suggest that the reaction system leaves the well (an H^- departs from SiH_4), and SiH_4 acquires a slight vibrational energy. However, these profiles

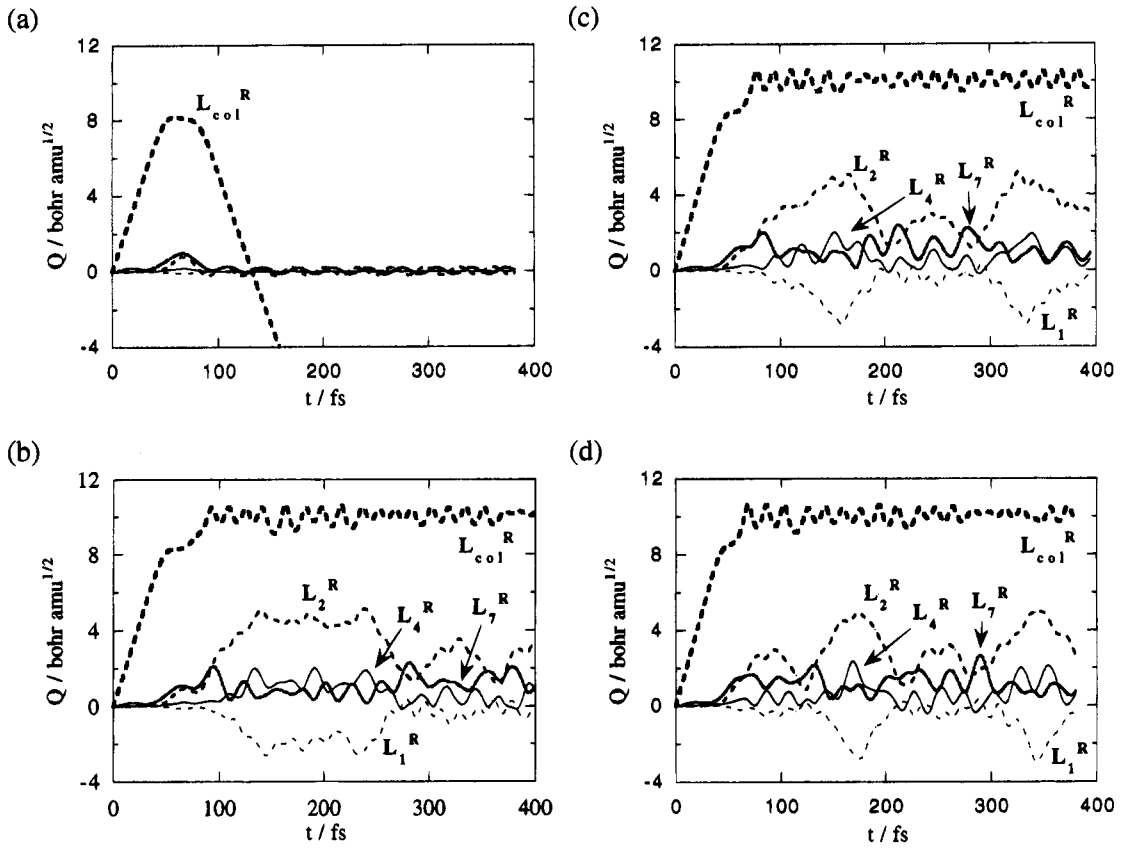

Figure 7. Changes of normal coordinates of the reactant along the DRC trajectory in side attack. Each part of (a)−(d) corresponds to parts (a)−(d) of Figure 6, respectively.

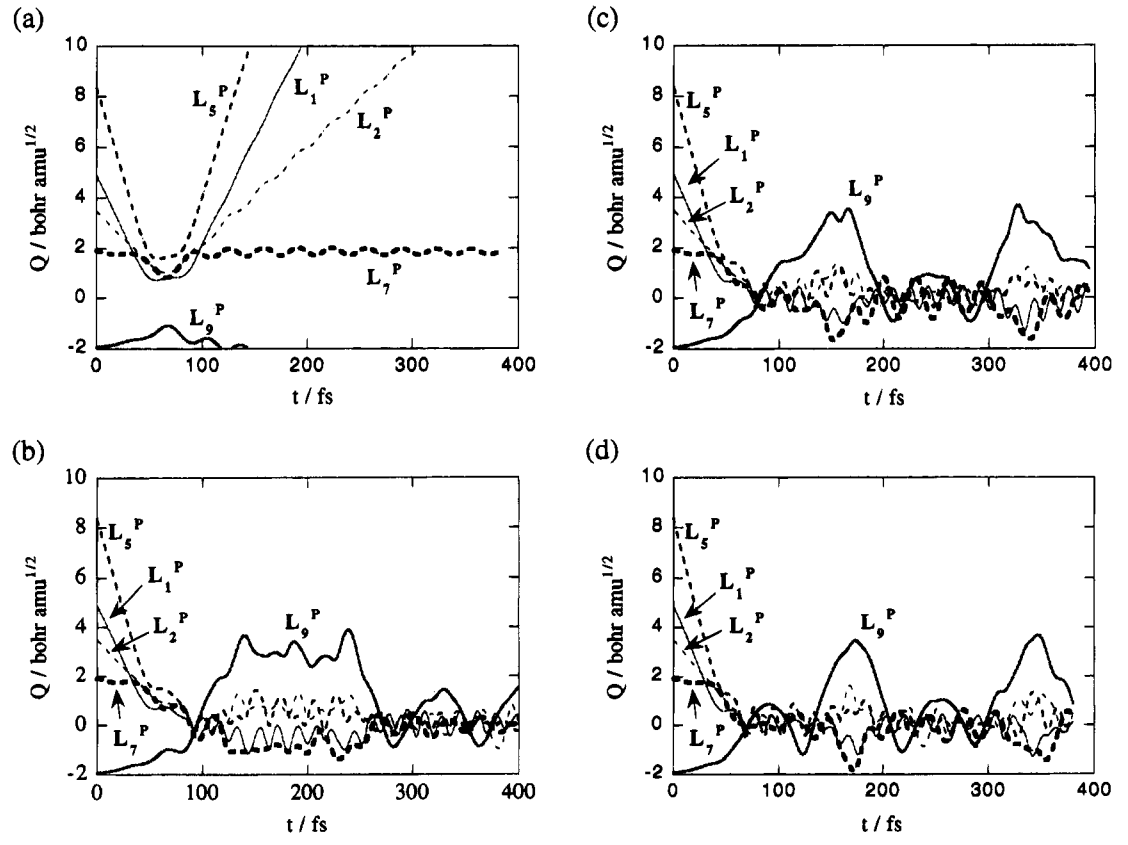

Figure 8. Changes of normal coordinates of the product along the DRC trajectory in side attack. Each part of (a)−(d) corresponds to parts (a)−(d) of Figure 6, respectively.

do not provide sufficient information to determine which H (the initial approaching H^- or an H in SiH_4) departs. This will be clear from our normal mode mapping analysis, discussed below.

Parts (a)−(d) of Figure 10 show fluctuations of the normal coordinates of the reactant along the DRC trajectories, corresponding to parts (a)−(d) of Figure 9, respectively. These

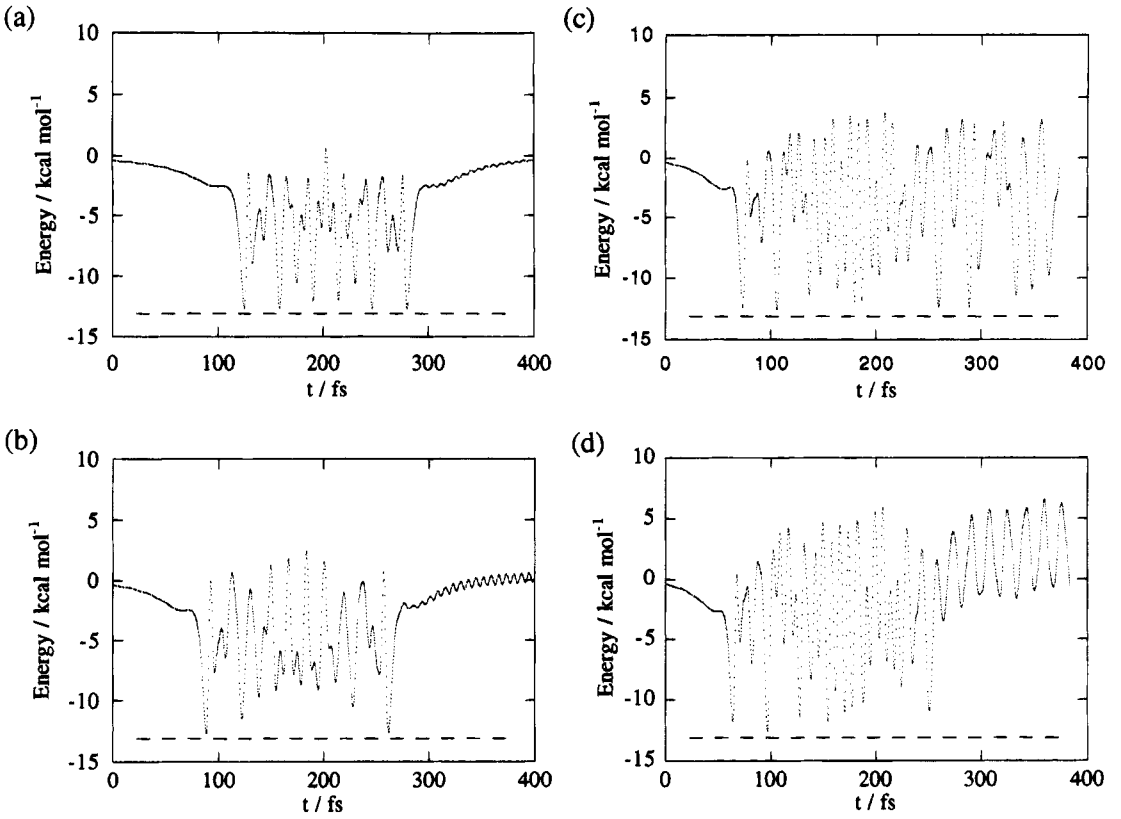

Figure 9. Potential energy changes along the DRC trajectory in front attack; the initial kinetic energy is (a) 1, (b) 3, (c) 5, and (d) 7 kcal/mol. The dashed line shows the potential energy well (global minimum).

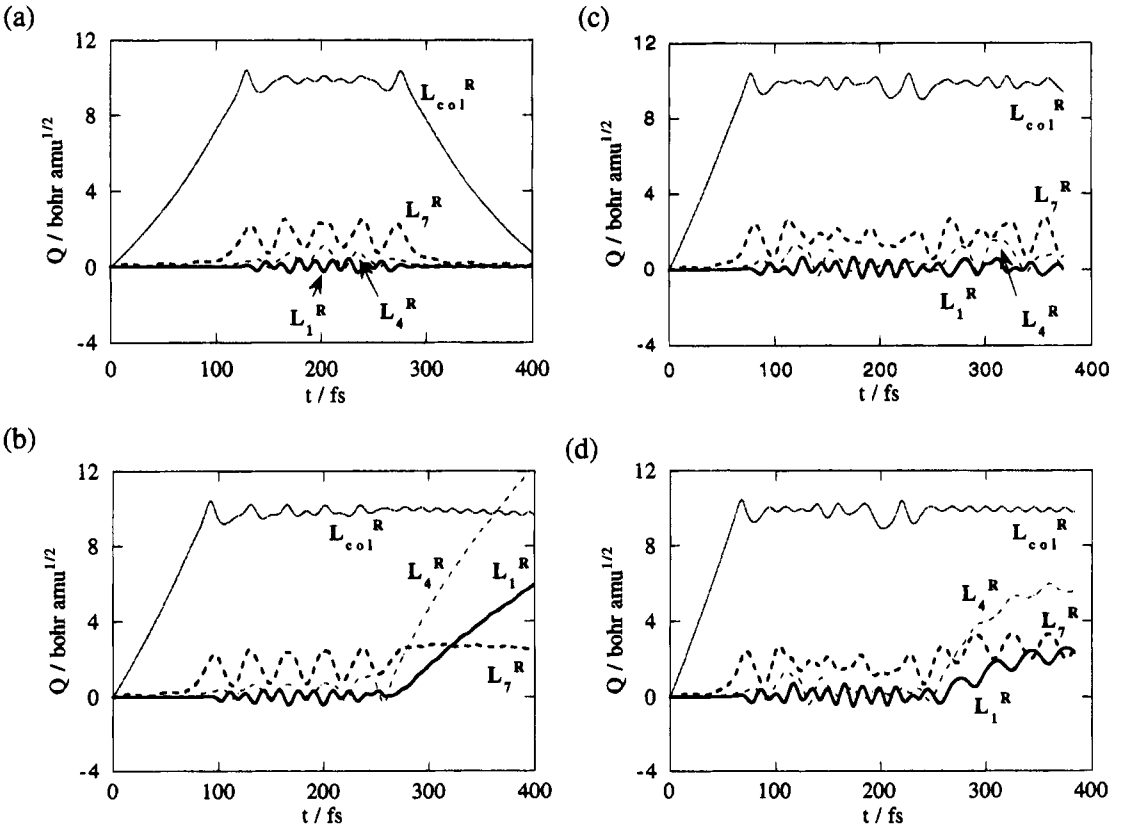

Figure 10. Changes of normal coordinates of the reactant along the DRC trajectory in front attack. Each part of (a)−(d) corresponds to parts (a)−(d) of Figure 9, respectively.

figures show that the reaction system goes in the direction of $\mathbf{L}_{col}^R$ initially. At $Q_{col}^R \approx 10$ bohr amu$^{1/2}$, the system enters the domain of SiH_5^- and the other modes start to fluctuate. In case (a), with just 1 kcal/mol kinetic energy, all coordinates except Q_{col}^R settle to zero after the initial fluctuations ($t > \sim 300$ fs) and Q_{col}^R decreases with a constant rate. These results suggest that with very small kinetic energy input, the initial approaching H^- is scattered through a dynamic interaction with

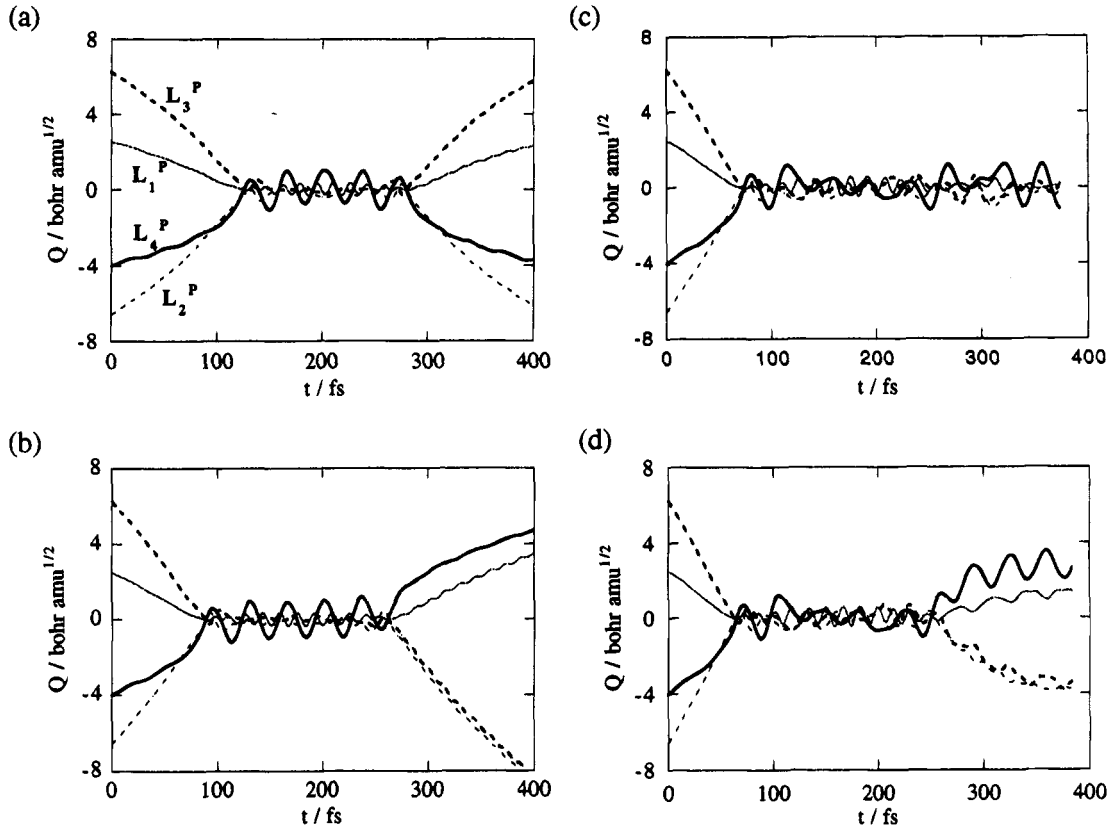

Figure 11. Changes of normal coordinates of the product along the DRC trajectory in front attack. Each part of (a)−(d) corresponds to parts (a)−(d) of Figure 9, respectively.

SiH_4 over 200 fs ($t \cong 100-300$ fs). When the starting kinetic energy is increased to ≥3 kcal/mol (parts (b)−(d) of Figure 10), different behavior is observed.

As described in the previous section, the characteristic modes leading to the S_N2 reaction are $\mathbf{L}_4^R$ and $\mathbf{L}_7^R$ in the reactant and $\mathbf{L}_4^P$ in the product. The $\mathbf{L}_7^R$ mode in Figure 5a corresponds to a reverse umbrella motion (H_3) in SiH_4. In equilibrium SiH_5^-, Si is located in the plane of the H_3 umbrella. Thus, as the H^- approaches SiH_4, the SiH_4 moiety feels a force in the positive $\mathbf{L}_7^R$ direction, resulting in vibrational excitation of the $\mathbf{L}_7^R$ mode. As shown in parts (b)−(d) of Figure 10, the reaction system undergoes a $\mathbf{L}_7^R$ vibrational motion at around $Q_7^R = 1.2$ bohr amu$^{1/2}$ at ~250 fs. This corresponds to the geometry of equilibrium SiH_5^-. Note that the movement of Q_4^R is in phase with that of Q_7^R. When the reaction system goes beyond the dissociation limit in $\mathbf{L}_7^R$, the system leaves the well of the product and the two fragments, *i.e.*, H^- and SiH_4, separate. When dissociation in $\mathbf{L}_7^R$ occurs in the positive phase, an S_N2 reaction occurs. When dissociation occurs in the negative phase, the approaching H^- is scattered. Thus, an S_N2 reaction occurs in case (b), while scattering occurs in case (a). In case (c), neither of these occurs during 400 fs. In case (d), an S_N2 reaction may occur, but there is still out-of-phase vibrational structure between $\mathbf{L}_1^R$ and $\mathbf{L}_7^R$. Thus, scattering of H^- is not complete, and H^- may still be bound to SiH_4.

Figure 11 illustrates changes in the normal coordinates of the product along the DRC trajectory, analogous to those just discussed for the reactant modes in Figure 10. The SiH_5^- complex is formed at about $t = 100$ fs. In case (a) (smallest kinetic energy), all coordinates return to their initial values at about $t = 400$ fs (scattering). In case (b), the reaction system leaves equilibrium SiH_5^- at about $t = 300$ fs, although Q_3^P and Q_4^P have changed their signs. This can be understood by examining Figure 5b; the two H atoms exchanged in the S_N2 reaction have antisymmetric motions in $\mathbf{L}_3^P$ and $\mathbf{L}_4^P$. In case (c), the reaction system remains within the SiH_5^- well over 400 fs. As expected, the fluctuation of the $\mathbf{L}_4^P$ mode is large. In case (d), the profiles are qualitatively similar to those for case (b) (the S_N2 reaction). However, the deviation of the coordinates from zero is very loose. In addition, each coordinate has some vibrational structure. This may indicate that the reaction system forms a loosely bound complex, exhibiting a large amplitude motion around the well.

For examination of the dynamics of the H^--SiH_4 complex in case (d), we performed DRC calculations over a much longer (1200 fs) time period. Figure 12 shows the resulting changes in the normal coordinates of (a) the reactant, (b) the product, and (c) changes in two Si−H distance, r_1 and r_2, along the DRC trajectory. Here, r_1 denotes the distance from the initial approaching H_a^- and r_2 denotes that from the H_d in the opposite side. These figures show that, although the complex attempts to separate into H^- and SiH_4 in a manner reminiscent of an S_N2 reaction, at about 250−400 fs, it cannot escape and returns to the product well. Note that H_d (r_2) lengthens to almost 5 Å away from Si at 390 fs. Around 1 ps, the complex again unsuccessfully attempts to escape the well.

In summary, either scattering of the approaching H^- or an S_N2 reaction may occur by a front attack with a small initial relative velocity. In some cases, this mode of attack forms a loosely bound complex around the SiH_5^- well.

IV. Conclusion

In this paper, dynamical aspects of the reaction $SiH_4 + H^- \rightarrow SiH_5^-$ are studied by the DRC method based on *ab initio* MO calculations. To clarify the energy transfer mechanism, the DRC and its conjugate momentum are mapped onto both reactant and product normal modes. This analysis shows that, under side attack, the initial translational energy is transferred to the $\mathbf{L}_9^P$ mode of SiH_5^- and Berry pseudorotation can occur

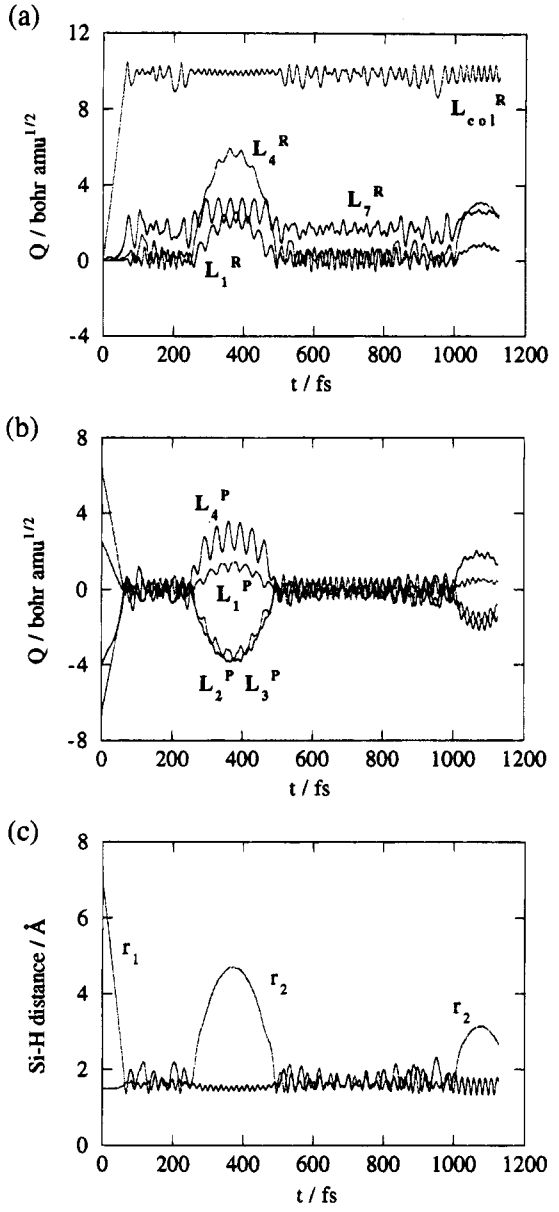

Figure 12. Changes in the normal coordinates of (a) the reactant and (b) the product, and (c) changes in two Si−H distances r_1 and r_2, along the DRC trajectory over 1200 fs for case d in Figure 9; r_1 denotes the distance from the initial approaching H^-; r_2 denotes the distance from the H in the opposite side.

continuously within the SiH_5^- well. Under front attack, scattering of the initial approaching H^- or an S_N2 reaction occurs, depending on the initial relative velocity. In some cases, the reaction system forms a loosely bound complex around the well.

Acknowledgment. This work was supported in part by grants from the National Science Foundation (CHE-9313717) and the Air Force Office of Scientific Research (93-0105). The calculations described here were performed on IBM RS 6000 work stations generously provided by Iowa State University. Suggestions made by Dr. Theresa Windus regarding the manuscript are gratefully acknowledged.

References and Notes

(1) Mutterties, E. L.; Guggenberger, L. J. *J. Am. Chem. Soc.* **1974**, *96*, 1748.
(2) Birgi, H. B. *Angew. Chem., Int. Ed. Engl.* **1975**, *14*, 460.
(3) Holmes, R. R.; Deiters, J. A. *J. Am. Chem. Soc.* **1977**, *99*, 3318.
(4) Holmes, R. R.; Day, R. O.; Chandrasekhar, V.; Holmes, J. M. *Inorg. Chem.* **1985**, *24*, 2009.
(5) Hajdasz, D. J.; Squires, R. R. *J. Am. Chem. Soc.* **1986**, *108*, 3139.
(6) Davis, L. P.; Burggraf, L. W.; Gordon, M. S.; Baldridge, K. K. *J. Am. Chem. Soc.* **1985**, *107*, 4415.
(7) Gordon, M. S.; Davis, L. P.; Burggraf, L. W.; Damrauer, R. *J. Am. Chem. Soc.* **1986**, *108*, 7889.
(8) Davis, L. P.; Burggraf, L. W.; Gordon, M. S. *J. Am. Chem. Soc.* **1988**, *110*, 3056.
(9) Damrauer, R.; Burggraf, L. W.; Davis, L. P.; Gordon, M. S. *J. Am. Chem. Soc.* **1988**, *110*, 6601.
(10) Gordon, M. S.; Davis, L. P.; Burggraf, L. W. *Chem. Phys. Lett.* **1989**, *163*, 371.
(11) Gordon, M. S.; Windus, T. L.; Burggraf, L. W.; Davis, L. P. *J. Am. Chem. Soc.* **1990**, *112*, 7167.
(12) Windus, T. L.; Gordon, M. S.; Burggraf, L. W.; Davis, L. P. *J. Am. Chem. Soc.* **1991**, *113*, 4356.
(13) Carroll, M. T.; Gordon, M. S.; Windus, T. L. *Inorg. Chem.* **1992**, *31*, 825.
(14) Windus, T. L.; Gordon, M. S. *Theor. Chim. Acta* **1992**, *83*, 21.
(15) Davis, L. P.; Burggraf, L. W.; Gordon, M. S. *Int. J. Quantum Chem.* **1992**, *44*, 691.
(16) Gordon, M. S.; Carroll, M. T.; Davis, L. P.; Burggraf, L. W. *Comput. Mater. Sci.* **1993**, *1*, 161.
(17) Windus, T. L.; Gordon, M. S.; Davis, L. P.; Burggraf, L. W. *J. Am. Chem. Soc.* **1994**, *116*, 3568.
(18) Berry, R. S. *J. Chem. Phys.* **1960**, *32*, 933.
(19) (a) Fukui, K. *J. Phys. Chem.* **1970**, *74*, 4161. (b) Ishida, K.; Morokuma, K.; Komornicki, A. *J. Chem. Phys.* **1977**, *66*, 2153. (c) Schmidt, M. W.; Gordon, M. S.; Dupuis, M. *J. Am. Chem. Soc.* **1985**, *107*, 2585. (d) Garrett, B. C.; Redmon, M. J.; Steckler, R.; Truhlar, D. G.; Baldridge, K. K.; Bartol, D.; Schmidt, M. W.; Gordon, M. S. *J. Phys. Chem.* **1988**, *92*, 1476. (e) Baldridge, K. K.; Gordon, M. S.; Steckler, R.; Truhlar, D. G. *J. Phys. Chem.* **1989**, *93*, 5107. (f) Gonzalez, C.; Schlegel, H. B. *J. Chem. Phys.* **1989**, *90*, 2154.
(20) Miller, W. H.; Handy, N. C.; Adams, J. E. *J. Chem. Phys.* **1980**, *72*, 99.
(21) Hirano, T.; Taketsugu, T.; Kurita, Y. *J. Phys. Chem.* **1994**, *98*, 6936.
(22) Hirano, T.; Taketsugu, T.; Kurita, Y. *J. Phys. Chem.* **1994**, *98*, 6942.
(23) Stewart, J. J. P.; Davis, L. P.; Burggraf, L. W. *J. Comput. Chem.* **1987**, *8*, 1117.
(24) Maluendes, S. A.; Dupuis, M. *J. Chem. Phys.* **1990**, *93*, 5902.
(25) Taketsugu, T.; Hirano, T. To be submitted.
(26) Dewar, M. J. S.; Thiel, W. *J. Am. Chem. Soc.* **1977**, *99*, 4899.
(27) Dupuis, M.; Farazdel, A.; Karna, S. P.; Maluendes, S. A. In *MOTEC: Modern Techniques in Computational Chemistry*; Clementi, E., Ed.; ESCOM, Leiden: The Netherlands, 1990; pp 277.
(28) Schmidt, M. W.; Baldridge, K. K.; Boatz, J. A.; Elbert, S. T.; Gordon, M. S.; Jensen, J. H.; Koseki, S.; Matsunaga, N.; Nguyen, K. A.; Su, S.; Windus, T. L.; Dupuis, M.; Montgomery, J. A. *J. Comput. Chem.* **1993**, *14*, 1347.
(29) (a) Helgaker, T.; Uggerund, E.; Jensen, H. J. A. *Chem. Phys. Lett.* **1990**, *173*, 145. (b) Uggerund, E.; Helgaker, T. *J. Am. Chem. Soc.* **1992**, *114*, 4265.
(30) Chen, W.; Hase, W. L.; Schlegel, B. *Chem. Phys. Lett.* **1994**, *228*, 436.
(31) Frisch, M. J.; Pople, J. A.; Binkley, J. S. *J. Chem. Phys.* **1984**, *80*, 4244.
(32) In this paper, all normal modes are represented in the mass-weighted coordinate.

JP950093K